• Clinical Research •

Repeatability, reproducibility, and agreement regarding measurement of choroidal vascularity index between OCT and OCT angiography

Mu-Han Zhong, Jia-Li Zhang, Ke-Xin Yu, Shu-Qi Fan, Xue Li, Hao Chen, Jin-Hua Bao, Ying-Ying Huang

National Engineering Research Center of Ophthalmology and Optometry, Eye Hospital, Wenzhou Medical University, Wenzhou 325027, Zhejiang Province, China

Co-first Authors: Mu-Han Zhong and Jia-Li Zhang

Correspondence to: Ying-Ying Huang and Jin-Hua Bao. National Engineering Research Center of Ophthalmology and Optometry, Eye Hospital, Wenzhou Medical University, 270 West Xueyuan Road, Wenzhou 325027, Zhejiang Province, China. huangyy@eye.ac.cn; baojessie@mail.eye.ac.cn

Received: 2025-07-26 Accepted: 2025-09-16

Abstract

● **AIM:** To explore the repeatability, reproducibility, and agreement in the measurement of the choroidal vascularity index (CVI) for different swept-source optical coherence tomography (OCT) devices and between OCT and OCT angiography (OCTA) images.

● **METHODS:** Two swept-source OCT imaging systems, VG200I and Topcon DRI OCT Triton, were used to capture OCT and OCTA images in triplicate. The first and third images were taken by one operator, and the second image was taken by another operator. The built-in software was used to calculate the CVI from the OCTA images (CVI-OCTA), and a custom-designed algorithm was used to calculate the CVI from the OCT images (CVI-OCT). Repeatability and reproducibility were assessed with the intraclass correlation coefficient (ICC), and agreement between devices and between OCT and OCTA were evaluated with Bland-Altman analysis.

● **RESULTS:** Sixty-eight eyes from 35 adults (17 females) were included in the analysis. The average age of the participants was 23.6±2.3y, with an average spherical equivalent refraction of -3.08±2.47 D and an average AL of 25.21±1.20 mm. Both OCT devices demonstrated high repeatability and reproducibility in measuring the CVI-OCTA (all ICCs>0.894 across five choroidal regions) and CVI-OCT (all ICCs>0.838). Furthermore, the between-device agreement in measuring the CVI-OCT was good [mean difference (MD) ranging from -2.32% to -3.07%], but that in measuring the CVI-OCTA was poor (MD, 1.48% to -7.43%). Additionally, the between-imaging agreement (CVI-OCTA versus CVI-OCT) was poor for both devices (Triton, MD, 6.05% to 12.68%; VG200I, MD, 6.67% to 12.09%).

● **CONCLUSION:** Both OCT devices and the two analytical methods demonstrate good stability. The inter-device consistency of CVI-OCT is good, while the inter-device consistency of CVI-OCTA and the consistency between the two analytical methods in the same device are both poor.

● **KEYWORDS:** choroidal vascularity index; optical coherence tomography angiography; agreement

DOI:10.18240/ijo.2026.03.10

Citation: Zhong MH, Zhang JL, Yu KX, Fan SQ, Li X, Chen H, Bao JH, Huang YY. Repeatability, reproducibility, and agreement regarding measurement of choroidal vascularity index between OCT and OCT angiography. *Int J Ophthalmol* 2026;19(3):498-508

INTRODUCTION

The choroid is an ocular tissue layer composed primarily of blood vessels. It is situated between the retina and the sclera and provides oxygen and nutrients to both. Changes in the choroidal vessels are associated with various eye and systemic diseases; decreased choroidal blood perfusion, for example, may lead to scleral hypoxia and contribute to an increase in axial length (AL), resulting in myopia[1], while patients with glaucoma and diabetes present with a decreased choroidal vascularity index (CVI)[2-3]. In patients with Parkinson's disease, the total choroidal area (TCA) and luminal area (LA) are larger, but the CVI is smaller than that in normal eyes[4]. Therefore, the CVI has received extensive attention in research and clinical practice in the management of ocular diseases.

In recent years, significant progress has been made in scanning-source optical coherence tomography (SS-OCT)[5-6], which uses infrared light for the high-resolution, cross-sectional 3D imaging of the posterior eye, helping to advance the study of

choroidal vascularity[7-9]. However, the results of choroidal vascularity assessment from different studies or different devices are not entirely consistent. Studies using different OCT instruments and analytical methods by Devarajan *et al*[10], Liu *et al*[11], and Wang *et al*[12] revealed inconsistent findings: the former two found no correlation between AL and CVI, while Wang *et al*[12] reported a negative correlation. In glaucoma research, Kee *et al*[13] detected significantly lower CVI in patients compared to healthy eyes using the RTVue device, whereas the Triton showed no intergroup differences. Additionally, both Querques *et al*[14] and Robbins *et al*[15] employed the AngioPlex device, with the former found no CVI differences between mild cognitive impairment and the normal population, but the latter noted reduced CVI in patients.

Consistency refers to the comparability of data obtained through repeated measurements with the same method across different instruments or with different analysis methods on the same instrument. Good consistency is essential for clinical follow-up and scientific research comparisons. Previous studies have measured the CVI with different image acquisition and analysis methods, potentially leading to differing results and unreliable clinical guidance. In this study, different OCT devices commonly used in recent studies were employed to evaluate the agreement, repeatability, and reproducibility related to CVI measurements from OCT and OCT angiography (OCTA) images.

PARTICIPANTS AND METHODS

Ethical Approval This cross-sectional study was approved by the Ethics Committee of the Eye Hospital of Wenzhou Medical University (Approval No.2023-030-K-24), and all work was carried out following the tenets of the Declaration of Helsinki. All participants signed an informed consent form.

Participants The inclusion criteria for the participants were as follows: 1) age between 18 and 40y; 2) best corrected visual acuity in both eyes better than 0.0 logMAR; 3) no eye drops used in the past month except for artificial tears; 4) no fundus lesions other than tessellated lesions.

Image Acquisition Images were captured with three devices in a random order: VG200I (Intalight, Henan, China), DRI OCT Triton (Topcon Corporation, Tokyo, Japan), and RTVue XR Avanti (Optovue Inc., Fremont, CA, USA). The RTVue is a spectral domain OCT (SD-OCT) device with a light wavelength of 1050 nm and a scanning speed of 70 000 A-scans per second. The VG200I is an SS-OCT/OCTA device with a central wavelength of 1050 nm and a scanning rate of 200 000 A-scans per second. The axial resolution is 3.8 μm, and the lateral resolution is 10 μm. OCT images are acquired in 18-line radial scanning mode centered on the fovea, with a depth of 4.2 mm and a length of 12 mm. OCTA images are obtain in 3×3 mm, 512 A-scans×512 B-scans mode, with each B-scan repeated 4 times. The DRI OCT Triton is another SS-OCT/OCTA device with a scanning speed of 100 000 A-scans per second and a central wavelength of 1050 nm. The axial resolution is 8 μm, and the lateral resolution is 20 μm. OCT images are obtained in a 12-line radial scanning mode centered on the fovea. The scanning depth is 2.6 mm, and the length is 9 mm. OCTA images of 3×3 mm are acquired with 320 A-scans×320 B-scans, and each B-scan is repeated 4 times. For this study, only the images acquired from the VG200I and Triton were included for CVI analysis, as the custom algorithm could not identify unclear choroidal boundaries on OCT images acquired from the RTVue, and its built-in software is unable to calculate the CVI from OCTA images[16].

The thickness of the choroid undergoes rhythmic changes, so the experiment time for each participant lasted no more than one hour, and all experiments took place between 9:00 and 17:00[17-18]. Before the experiment, participants watched movies for 20min in a dark environment, 4 m away from the television (97.5×64 cm), with both eyes adequately corrected to eliminate the impact of previous near work on the choroid. The experiment was conducted by two operators: operator 1 took the first and third measurements, while operator 2 took the second measurement. The first and third measurements were compared to assess reproducibility, and the first and second measurements were compared to assess repeatability. The operators received specialized training on the study protocol and were required to ensure clear focus and the absence of motion artifacts. OCT images were included only if they scored over 8 (VG200I) or 94 (Triton) points, and OCTA scan results were included only if they scored over 8 (VG200I) or 60 (Triton) points. The image magnification was corrected by inputting the individual AL, which was measured by a Lenstar LS 900 (Haag Streit, Koeniz, Switzerland) before the OCT measurements were acquired.

Choroidal Parameter Analysis An image analysis method developed based on MATLAB R2017a (MathWorks, Natick, MA, USA) and Python was used for quantitative analysis of the choroid parameters in OCT images. First, the residual U-Net model was used to segment the choroidal boundaries to extract the region of interest (ROI). The ROI was then converted into an RGB image, and the Niblack local threshold algorithm was applied for image binarization, where the black pixel area was identified as the vascular LA, and the white pixel area was determined as the stromal area (SA). Finally, MATLAB was used for pixel counting, and the pixel counts were converted into actual physical areas (mm^2) based on the image resolution to obtain quantitative data for TCA, LA, and SA (Figure 1A-1D). This integrated method combines the advantages of deep learning segmentation and local adaptive

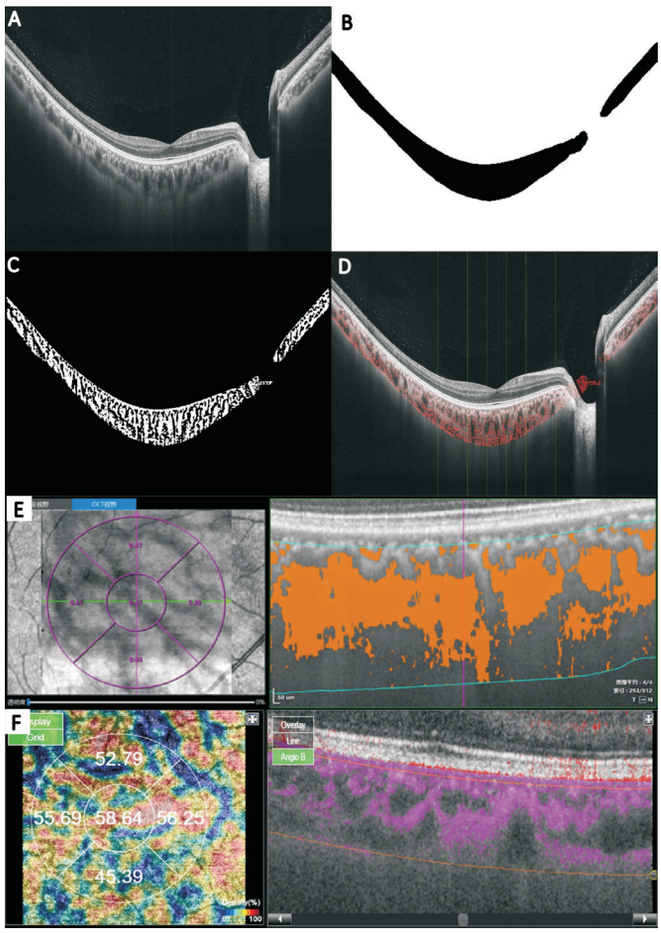

Figure 1 Diagram of choroidal vascular analysis with the custom algorithm A: Original image; B: Choroidal boundary segmentation; C: Image binarization; D: Binarized image and choroid boundary segmentation corresponding to the original images; E: CVI analysis by the built-in software of the VG200I; F: CVI analysis by the built-in software of the Triton. CVI: Choroidal vascularity index.

threshold algorithms to achieve precise quantitative analysis of choroidal structures[16,19]. The CVI was defined as the ratio of the LA to the TCA[20]. The CVI from OCT images, defined as CVI-OCT, represents the CVI of medium and large vessels between 20 μm below the RPE-Bruch's membrane complex and the bottom boundary of the choroid[21]. The 3D synthesis of LA, SA, and TCA was obtained by combining all the images from a radial scan. Since the Triton obtains 12 OCT images from a single radial scan, while the VG200I obtains 18 images, the result from the Triton-acquired images was further multiplied by 1.5. The 3D synthesis of the CVI was obtained by averaging the CVI of all images obtained from a single radial scan. According to the Early Treatment Diabetic Retinopathy Study (ETDRS)[22], the central 3×3 mm circular area on the OCT images was divided into five regions: the 1 mm central zone (C), the nasal zone between 1 and 3 mm (N), the superior zone between 1 and 3 mm (S), the temporal zone between 1 and 3 mm (T), the and inferior zone between 1 and 3 mm (I).

The built-in software designed for analyzing the CVI from OCTA images by the manufacturers of the two devices was used to calculate CVI-OCTA. The upper and lower boundaries of the choroid were consistent among the OCT images, *i.e.*, between approximately 20 μm below the RPE-Bruch's membrane complex and the bottom boundary of the choroid. The CVI-OCTA in the five ETDRS regions was obtained directly from the built-in software (Figure 1E-1F).

Statistical Analysis SPSS 26.0 (IBM Corp., Armonk, NY, USA) was used for statistical analysis. The Kolmogorov-Smirnov test was used for assessing the normality of the data. Repeatability and reproducibility were estimated with the intraclass correlation coefficient (ICC) and coefficient of variation (CV). Bland-Altman plots and paired *t*-tests were used to assess the consistency in the measurements between the two devices and the two types of image. Additionally, Pearson or Spearman correlation analysis was used to assess the correlation between AL and the CVI. A *P* value of less than 0.05 was considered to indicate statistical significance. All the results are presented as the means±standard deviations (SDs).

RESULTS

In this cross-sectional study, 37 healthy adult subjects (74 eyes) were initially recruited, but 6 eyes were excluded because of poor imaging quality. Ultimately, 68 eyes from 35 subjects (17 females) were included in the analysis. The average age of the participants was 23.6±2.3y, with an average spherical equivalent refraction of -3.08±2.47 D and an average AL of 25.21±1.20 mm.

Repeatability and Reproducibility Regarding the repeatability of the CVI results, the ICC values of the CVI-OCTA for the five regions for the VG200I ranged from 0.959 to 0.977, and those of the CVI-OCT ranged from 0.838 to 0.931 (Table 1). For the Triton, the ICC values of the CVI-OCTA ranged from 0.896 to 0.927, and those of the CVI-OCT ranged from 0.907 to 0.965 (Table 1). All the ICC values of the LA, SA, and TCA from the OCT images for the VG200I and Triton were greater than 0.986 (Table 2).

Regarding the reproducibility of the two devices, the ICC values of the CVI-OCTA for the VG200I ranged from 0.929 to 0.972, and those of the CVI-OCT ranged from 0.882 to 0.944 (Table 1). For the Triton, the ICC values of the CVI-OCTA ranged from 0.894 to 0.952, and those of the CVI-OCT ranged from 0.901 to 0.955 (Table 1). All the ICC values of the LA, SA and TCA were greater than 0.984 (Table 2).

Agreement Between-Device and Between-Imaging Comparison Table 3 displays the differences in the CVI-OCT and CVI-OCTA values obtained by the two devices (Figure 2). The ICC of the agreement in the CVI-OCTA ranged from -0.308 to -0.004; the values obtained from the VG200I were lower than those from the Triton, with 95%

Table 1 Repeatability and reproducibility data for the VG200I and Triton

Parameters	Repeatability				Reproducibility			
	VG200I		Triton		VG200I		Triton	
	ICC (95%CI)	CV (%)	ICC (95%CI)	CV (%)	ICC (95%CI)	CV (%)	ICC (95%CI)	CV (%)
CVI-OCTA								
Central	0.974 (0.958–0.984)	0.20	0.927 (0.885–0.954)	0.14	0.955 (0.928–0.972)	0.20	0.952 (0.924–0.970)	0.14
Nasal	0.977 (0.962–0.985)	0.23	0.926 (0.883–0.954)	0.14	0.931 (0.890–0.957)	0.24	0.938 (0.901–0.961)	0.14
Superior	0.959 (0.934–0.975)	0.19	0.917 (0.868–0.948)	0.13	0.929 (0.887–0.956)	0.19	0.933 (0.895–0.958)	0.13
Temporal	0.965 (0.944–0.978)	0.18	0.927 (0.885–0.954)	0.11	0.949 (0.918–0.968)	0.18	0.944 (0.911–0.965)	0.12
Inferior	0.972 (0.956–0.983)	0.18	0.896 (0.837–0.935)	0.14	0.972 (0.956–0.983)	0.18	0.894 (0.833–0.933)	0.14
CVI-OCT								
Central	0.931 (0.890–0.957)	0.03	0.965 (0.945–0.979)	0.05	0.944 (0.910–0.965)	0.03	0.955 (0.928–0.972)	0.05
Nasal	0.884 (0.818–0.927)	0.03	0.943 (0.909–0.964)	0.04	0.900 (0.843–0.937)	0.03	0.935 (0.897–0.959)	0.04
Superior	0.894 (0.834–0.933)	0.03	0.920 (0.874–0.950)	0.04	0.892 (0.831–0.932)	0.03	0.909 (0.857–0.943)	0.04
Temporal	0.838 (0.750–0.897)	0.03	0.909 (0.856–0.943)	0.04	0.882 (0.815–0.925)	0.03	0.910 (0.857–0.944)	0.04
Inferior	0.921 (0.875–0.950)	0.03	0.907 (0.853–0.941)	0.04	0.926 (0.883–0.954)	0.03	0.901 (0.861–0.945)	0.04

Central: 1 mm central zone; Nasal: Nasal zone between 1 and 3 mm; Superior: Superior zone between 1 and 3 mm; Temporal: Temporal zone between 1 and 3 mm; Inferior: Inferior zone between 1 and 3 mm; CVI-OCTA: Choroidal vascularity index calculated with the OCT built-in software on OCTA images; CVI-OCT: Choroidal vascularity index calculated with the custom-designed algorithm on OCT images; ICC: Intraclass correlation coefficient; CI: Confidence interval; CV: Coefficient of variation; OCT: Optical coherence tomography; OCTA: OCT angiography.

Table 2 Repeatability and reproducibility of the LA, SA and TCA measured from OCT images with the VG200I and Triton

Parameters	Repeatability				Reproducibility			
	VG200I		Triton		VG200I		Triton	
	ICC (95%CI)	CV (%)	ICC (95%CI)	CV (%)	ICC (95%CI)	CV (%)	ICC (95%CI)	CV (%)
LA-OCT								
Central	0.996 (0.994–0.998)	0.22	0.994 (0.990–0.996)	0.29	0.996 (0.994–0.998)	0.27	0.994 (0.990–0.996)	0.29
Nasal	0.997 (0.995–0.998)	0.28	0.994 (0.991–0.996)	0.32	0.998 (0.996–0.999)	0.30	0.992 (0.987–0.995)	0.32
Superior	0.995 (0.991–0.997)	0.26	0.994 (0.991–0.996)	0.27	0.995 (0.992–0.997)	0.26	0.995 (0.991–0.997)	0.27
Temporal	0.996 (0.993–0.998)	0.24	0.986 (0.977–0.991)	0.26	0.996 (0.994–0.998)	0.24	0.984 (0.974–0.990)	0.26
Inferior	0.997 (0.996–0.998)	0.28	0.995 (0.991–0.997)	0.29	0.997 (0.995–0.998)	0.28	0.995 (0.992–0.997)	0.29
SA-OCT								
Central	0.995 (0.992–0.997)	0.29	0.993 (0.989–0.996)	0.33	0.995 (0.991–0.997)	0.29	0.994 (0.990–0.996)	0.33
Nasal	0.996 (0.993–0.997)	0.31	0.991 (0.985–0.994)	0.34	0.994 (0.991–0.997)	0.31	0.989 (0.983–0.993)	0.34
Superior	0.993 (0.998–0.996)	0.26	0.991 (0.985–0.994)	0.29	0.993 (0.998–0.996)	0.26	0.992 (0.987–0.995)	0.29
Temporal	0.995 (0.993–0.997)	0.26	0.988 (0.980–0.992)	0.29	0.994 (0.990–0.996)	0.26	0.985 (0.975–0.990)	0.29
Inferior	0.995 (0.992–0.997)	0.28	0.993 (0.988–0.995)	0.33	0.994 (0.989–0.996)	0.28	0.995 (0.991–0.997)	0.33
TCA-OCT								
Central	0.997 (0.996–0.998)	0.28	0.995 (0.991–0.997)	0.30	0.996 (0.993–0.997)	0.28	0.995 (0.992–0.997)	0.30
Nasal	0.998 (0.997–0.999)	0.31	0.994 (0.991–0.996)	0.32	0.997 (0.996–0.998)	0.31	0.993 (0.988–0.995)	0.32
Superior	0.996 (0.993–0.997)	0.26	0.995 (0.992–0.997)	0.27	0.995 (0.992–0.997)	0.26	0.995 (0.993–0.997)	0.28
Temporal	0.998 (0.996–0.999)	0.25	0.989 (0.982–0.993)	0.27	0.997 (0.995–0.998)	0.25	0.986 (0.978–0.991)	0.27
Inferior	0.998 (0.996–0.998)	0.28	0.996 (0.993–0.997)	0.31	0.996 (0.994–0.998)	0.28	0.998 (0.996–0.999)	0.31

Central: 1 mm central zone; Nasal: Nasal zone between 1 and 3 mm; Superior: Superior zone between 1 and 3 mm; Temporal: Temporal zone between 1 and 3 mm; Inferior: Inferior zone between 1 and 3 mm; LA-OCT: Choroidal vascular luminal area calculated with the custom-designed algorithm on the OCT images; SA-OCT: Choroidal vascular stromal area calculated with the custom-designed algorithm on the OCT images; TCA-OCT: Total choroidal area calculated with the custom-designed algorithm on the OCT images; ICC: Intraclass correlation coefficient; CI: Confidence interval; CV: Coefficient of variation; OCT: Optical coherence tomography; OCTA: OCT angiography.

limits of agreement (LoA) ranging from -7.43 t o 1.48. For the CVI, LA, SA, and TCA obtained from OCT images, the ICCs of the agreements between devices ranged from 0.288 to 0.992. The 95% LoA for the CVI-OCT ranged from -2.32 to -3.07,

Table 3 Agreement between the VG200I and Triton mean±SD, %

Parameters	VG200I	Triton	95% LoA	ICC (95%CI)	[a]*P*
CVI-OCTA					
Central	47.55±9.46	54.99±7.33	-7.43 (-33.58 to 18.72)	-0.178 (-0.378 to 0.051)	<0.001
Nasal	46.29±10.35	51.41±6.78	-5.00 (-32.75 to 22.75)	-0.258 (-0.460 to 0.026)	<0.001
Superior	45.60±8.50	47.37±6.16	-1.70 (-22.37 to 18.98)	-0.004 (-0.237 to 0.231)	0.187
Temporal	50.08±8.54	51.87±5.92	-1.57 (-25.17 to 22.04)	-0.308 (-0.509 to -0.075)	0.182
Inferior	50.72±9.16	49.46±6.59	1.48 (-22.25 to 25.21)	-0.142 (-0.367 to 0.099)	0.334
CVI-OCT					
Central	58.40±1.88	61.03±2.73	-2.63 (-5.81 to 0.54)	0.456 (-0.099 to 0.768)	<0.001
Nasal	58.51±1.66	61.08±2.58	-2.58 (-5.44 to 0.29)	0.455 (-0.095 to 0.774)	<0.001
Superior	57.73±1.46	60.05±2.17	-2.32 (-5.02 to 0.38)	0.405 (-0.099 to 0.732)	<0.001
Temporal	58.09±1.46	61.13±2.19	-3.04 (-6.00 to -0.08)	0.288 (-0.085 to 0.633)	<0.001
Inferior	57.62±1.69	60.69±2.47	-3.07 (-6.41 to 0.26)	0.331 (-0.094 to 0.671)	<0.001

[a]Paired *t*-test. Central: 1 mm central zone; Nasal: Nasal zone between 1 and 3 mm; Superior: Superior zone between 1 and 3 mm; Temporal: Temporal zone between 1 and 3 mm; Inferior: Inferior zone between 1 and 3 mm; CVI-OCTA: Choroidal vascularity index calculated with the OCT built-in software on the OCTA images; CVI-OCT: Choroidal vascularity index calculated with the custom-designed algorithm on the OCT images; SD: Standard deviation; LoA: Limits of agreement; ICC: Intraclass correlation coefficient; CI: Confidence interval; OCT: Optical coherence tomography; OCTA: OCT angiography.

Table 4 Agreement in the LA, SA and TCA measured from OCT images between the VG200I and Triton mean±SD, mm^2

Parameters	VG200I	Triton	95% LoA	ICC (95%CI)	[a]*P*	[b]*r*	[b]*P*
LA-OCT							
Central	3.12±0.86	3.07±0.88	0.051 (-0.180 to 0.282)	0.989 (0.979 to 0.994)	<0.001	0.991	<0.001
Nasal	1.43±0.44	1.43±0.46	-0.003 (-0.112 to 0.106)	0.992 (0.987 to 0.995)	0.666	0.993	<0.001
Superior	1.55±0.40	1.56±0.42	-0.005 (-0.121 to 0.111)	0.990 (0.983 to 0.994)	0.47	0.990	<0.001
Temporal	1.60±0.39	1.59±0.41	0.013 (-0.131 to 0.157)	0.983 (0.972 to 0.989)	0.145	0.984	<0.001
Inferior	1.54±0.43	1.52±0.44	0.021 (-1.005 to 1.048)	0.991 (0.983 to 0.995)	0.01	0.990	<0.001
SA-OCT							
Central	2.22±0.08	1.97±0.65	0.251 (0.048 to 0.454)	0.917 (-0.005 to 0.981)	<0.001	0.987	<0.001
Nasal	1.02±0.39	0.92±0.32	0.098 (0.012 to 0.184)	0.946 (0.045 to 0.987)	<0.001	0.991	<0.001
Superior	1.07±0.04	1.04±0.30	0.098 (-0.008 to 0.205)	0.933 (0.088 to 0.983)	<0.001	0.984	<0.001
Temporal	1.16±0.04	1.02±0.31	0.139 (0.014 to 0.265)	0.883 (-0.022 to 0.971)	<0.001	0.978	<0.001
Inferior	1.13±0.04	0.99±0.33	0.138 (0.023 to 0.254)	0.902 (-0.015 to 0.977)	<0.001	0.985	<0.001
TCA-OCT							
Central	5.45±1.63	5.14±1.61	0.313 (0.066 to 0.691)	0.975 (0.414 to 0.994)	<0.001	0.990	<0.001
Nasal	2.50±0.83	2.40±0.83	0.099 (-0.060 to 0.257)	0.988 (0.830 to 0.997)	<0.001	0.992	<0.001
Superior	2.75±0.81	2.65±0.80	0.097 (-0.097 to 0.291)	0.985 (0.888 to 0.995)	<0.001	0.986	<0.001
Temporal	2.82±0.77	2.66±0.77	0.159 (-0.101 to 0.418)	0.965 (0.613 to 0.989)	<0.001	0.981	<0.001
Inferior	2.73±0.82	2.56±0.81	0.167 (-0.061 to 0.394)	0.970 (0.478 to 0.992)	<0.001	0.990	<0.001

[a]Paired *t*-test; [b]Pearson or Spearman analysis. LA-OCT: Choroidal vascular luminal area calculated with the custom-designed algorithm on the OCT images; SA-OCT: Choroidal vascular stromal area calculated with the custom-designed algorithm on the OCT images; TCA-OCT: Total choroidal area calculated with the custom-designed algorithm on the OCT images; Central: 1 mm central zone; Nasal: Nasal zone between 1 and 3 mm; Superior: Superior zone between 1 and 3 mm; Temporal: Temporal zone between 1 and 3 mm; Inferior: Inferior zone between 1 and 3 mm; SD: Standard deviation; LoA: Limits of agreement; ICC: Intraclass correlation coefficient; CI: Confidence interval; CV: Coefficient of variation; OCT: Optical coherence tomography; OCTA: OCT angiography.

while those for the LA, SA, and TCA ranged from -0.005 to 0.313 (Tables 3 and 4; Figure 2).

The ICC for the consistency between the two analytical methods for the VG200I and Triton ranged from -0.129 to 0.099 (Table 5). The mean values of the CVI-OCT were greater than those of CVI-OCTA, with 95% LoA ranging from -12.09 to -6.67 for the VG200I and from -12.68 to -6.05 for the Triton (Table 5 and Figure 3).

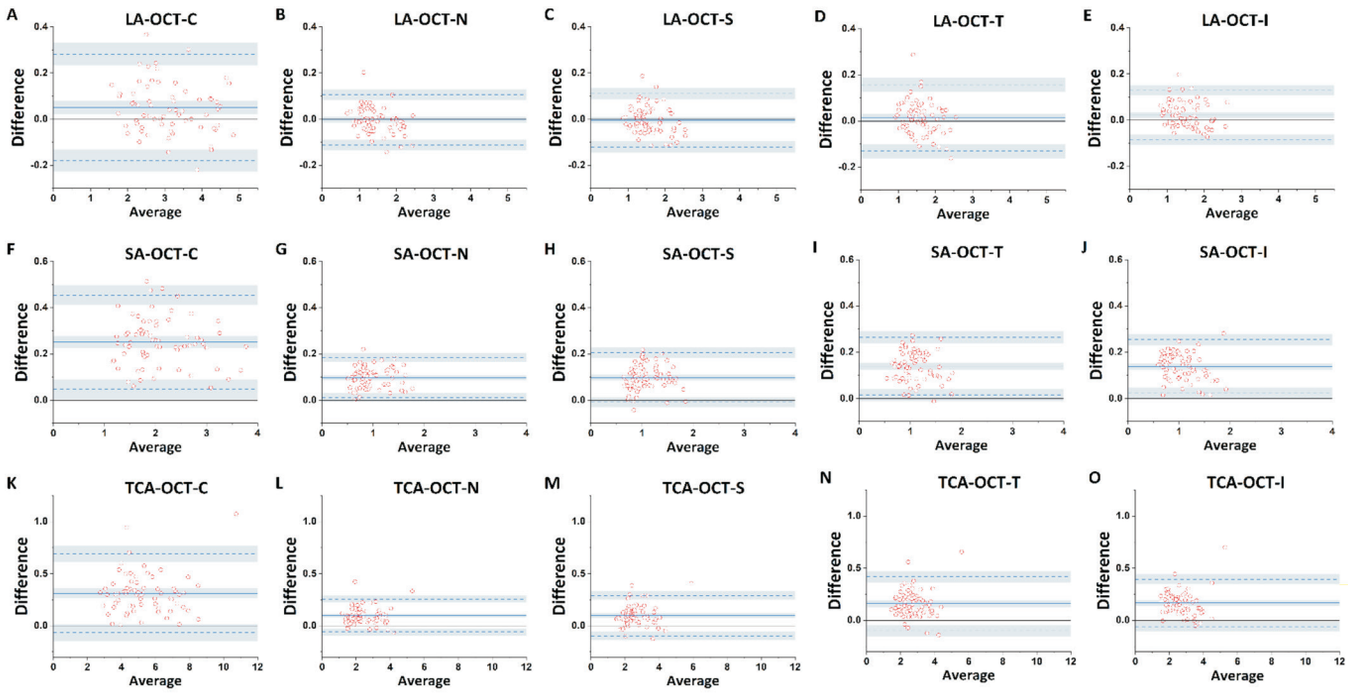

Figure 2 Bland-Altman plots of agreement in the LA-OCT, SA-OCT and TCA-OCT between the VG200I and Triton A-E: Bland-Altman plots of agreement for the LA-OCT between the VG200I and Triton; F-J: Bland-Altman plots of agreement in the SA-OCT between VG200I and Triton; K-O: Bland-Altman plots of agreement in the TCA-OCT between the VG200I and Triton. -C: 1 mm central zone; -N: Nasal zone between 1 and 3 mm; -S: Superior zone between 1 and 3 mm; -T: Temporal zone between 1 and 3 mm; -I: Inferior zone between 1 and 3 mm; LA-OCT: Luminal area calculated with the custom-designed algorithm on the OCT images; SA-OCT: Stromal area calculated with the custom-designed algorithm on the OCT images; TCA-OCT: Total area of choroid calculated with the custom-designed algorithm on the OCT images; OCT: Optical coherence tomography. The solid blue line indicates the average mean difference, and the dotted lines indicate the 95% limits of agreement.

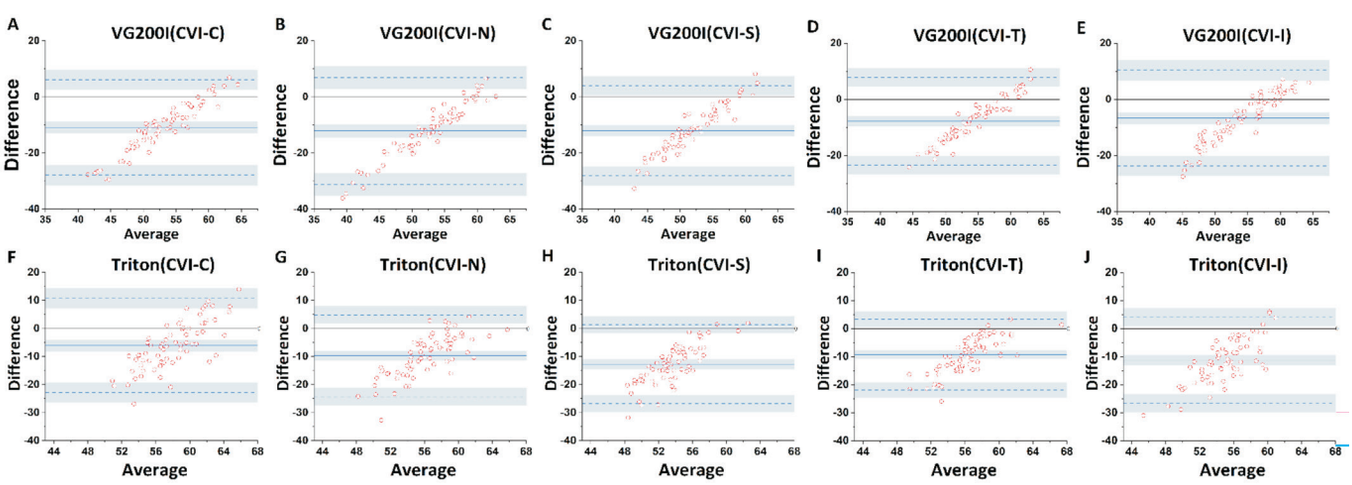

Figure 3 Bland-Altman plots of agreement between the CVI-OCTA and CVI-OCT A-E: Bland-Altman plots of agreement between the CVI-OCTA and CVI-OCT with the VG200I; F-J: Bland-Altman plots of agreement between the CVI-OCTA and CVI-OCT with the Triton. -C: 1 mm central zone; -N: Nasal zone between 1 and 3 mm; -S: Superior zone between 1 and 3 mm; -T: Temporal zone between 1 and 3 mm; -I: Inferior zone between 1 and 3 mm; CVI-OCTA: Choroidal vascularity index calculated with the built-in OCT software on the OCTA images; CVI-OCT: Choroidal vascularity index calculated with the custom-designed algorithm on the OCT images; OCT: Optical coherence tomography; OCTA: OCT angiography. The solid blue line indicates the average mean difference, the dotted lines indicate 95% limits of agreement, and the solid black line indicates zero.

The differences between the CVI-OCTA and CVI-OCT were positively correlated with the mean values (r ranging from 0.747 to 0.950, all P<0.001; Figure 3). When the CVI was greater, the difference between the two values was greater for both devices. The difference in the value of the CVI between the VG200I and Triton was strongly negatively correlated

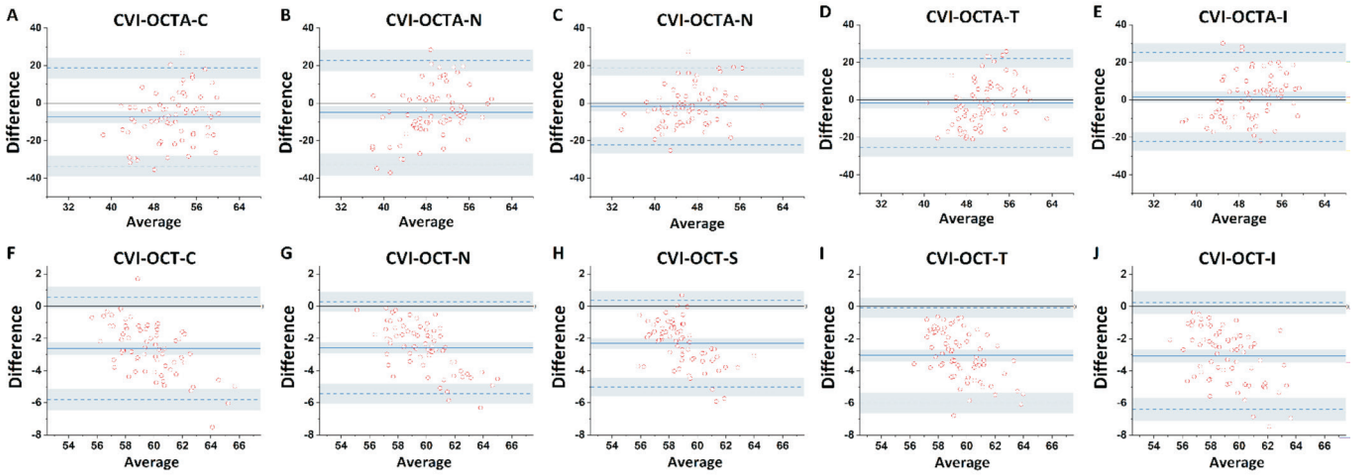

Figure 4 Bland-Altman plots of agreement in the CVI-OCTA and CVI-OCT between the VG200I and Triton A-E: Bland-Altman plots of agreement in the CVI-OCTA between the VG200I and Triton; F-J: Bland-Altman plots of agreement in the CVI-OCT between VG200I and Triton. -C: 1 mm central zone; -N: Nasal zone between 1 and 3 mm; -S: Superior zone between 1 and 3 mm; -T: Temporal zone between 1 and 3 mm; -I: Inferior zone between 1 and 3 mm; CVI-OCTA: Choroidal vascularity index calculated with the built-in OCT software on the OCTA images; CVI-OCT: Choroidal vascularity index calculated with the custom-designed algorithm on the OCT images; OCT: Optical coherence tomography; OCTA: OCT angiography. The solid blue line indicates the average mean difference, the dotted lines indicate the 95% limits of agreement, and the solid black line indicates zero.

Table 5 Agreement between the two analysis methods mean±SD, %

Parameters	CVI-OCTA	CVI-OCT	95% LoA	ICC (95%CI)	[a]*P*
VG200I					
Central	47.55±9.46	58.40±1.78	-10.85 (-27.87 to 6.18)	0.082 (-0.068 to 0.255)	<0.001
Nasal	46.29±10.35	58.51±1.66	-12.09 (-31.14 to 6.95)	0.067 (-0.066 to 0.226)	<0.001
Superior	45.60±8.50	57.73±1.46	-12.06 (-28.16 to 4.03)	0.035 (-0.055 to 0.153)	<0.001
Temporal	50.08±8.54	58.09±1.46	-7.79 (-23.50 to 7.93)	0.099 (-0.070 to 0.284)	<0.001
Inferior	50.72±9.16	57.62±1.69	-6.67 (-23.74 to 10.39)	0.091 (-0.079 to 0.277)	<0.001
Triton					
Central	54.99±7.33	61.03±2.73	-6.05 (-22.87 to 10.78)	-0.129 (-0.309 to 0.083)	<0.001
Nasal	51.41±6.78	61.08±2.58	-9.67 (-24.25 to 4.91)	-0.018 (-0.098 to 0.089)	<0.001
Superior	47.37±6.16	60.05±2.17	-12.68 (-26.73 to 1.36)	-0.043 (-0.120 to 0.085)	<0.001
Temporal	51.87±5.92	61.13±2.19	-9.26 (-21.91 to 3.40)	-0.015 (-0.084 to 0.081)	<0.001
Inferior	49.46±6.59	60.69±2.47	-11.23 (-26.53 to 4.07)	-0.065 (-0.171 to 0.104)	<0.001

[a]Paired *t*-test. Central: 1 mm central zone; Nasal: Nasal zone between 1 and 3 mm; Superior: Superior zone between 1 and 3 mm; Temporal: Temporal zone between 1 and 3 mm; Inferior: Inferior zone between 1 and 3 mm; CVI-OCTA: Choroidal vascularity index calculated by OCT built-in software in the OCTA images; CVI-OCT: Choroidal vascularity index calculated by the custom-designed algorithms in the OCT images; SD: Standard deviation; LoA: Limits of agreement; ICC: Intraclass correlation coefficient; CI: Confidence interval; OCT: Optical coherence tomography; OCTA: OCT angiography.

with the mean value of the CVI-OCT (*r* ranged from -0.472 to -0.660, all *P*<0.001; Figure 4) and positively correlated with the mean value of the CVI-OCTA (*r* ranged from 0.251 to 0.411; Figure 4). When the CVI was greater, the difference between the two devices was smaller for the CVI-OCT but greater for the CVI-OCTA.

Correlation Analysis Figure 5 shows the correlation analysis between the AL and CVI in the central region. Only the CVI-OCTA obtained with the Triton (*r*=0.551, *P*<0.001) was positively correlated with AL. However, neither the CVI-OCTA obtained with the VG200I device nor the CVI-OCT obtained from either device were correlated with AL. Furthermore, the LA, SA, and TCA in the central region obtained from the OCT images were negatively correlated with AL (Pearson's *r* ranged from -0.557 to -0.419, *P*<0.001; Figure 6).

DISCUSSION

The VG200I and Triton are widely used OCT devices in clinical practice and scientific research. For quantitatively analyzing images collected by the VG200I, custom software is generally preferred, whereas the Triton offers both custom and built-in software[21,23-31]. The results of this study revealed that the CVI obtained by the VG200I and Triton had good

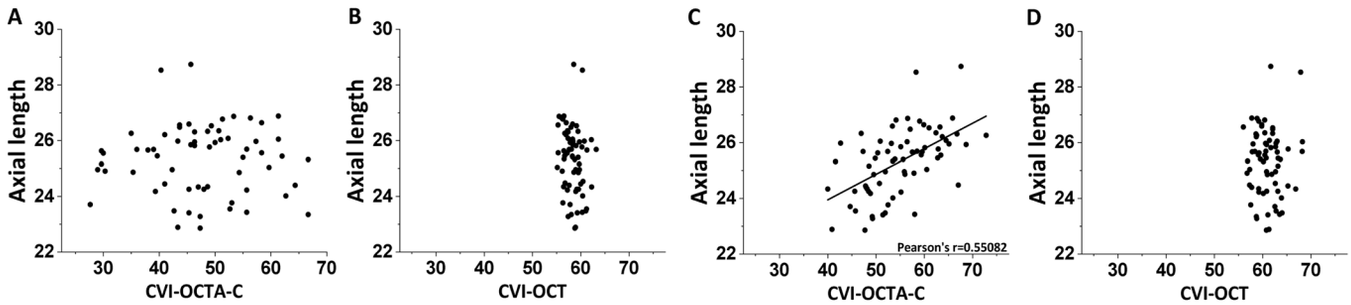

Figure 5 Scatter plots and fitting lines showing correlations between axial length (AL) and CVI values A: Correlation between AL and CVI-OCTA from the VG200I; B: Correlation between AL and CVI-OCT from the VG200I; C: Correlation between AL and CVI-OCTA from the Triton; D: Correlation between AL and CVI-OCT from the Triton. CVI-OCTA: Choroidal vascularity index calculated by the built-in OCT software on the OCTA images; CVI-OCT: Choroidal vascularity index calculated by the custom-designed algorithm on the OCT images; OCT: Optical coherence tomography; OCTA: OCT angiography.

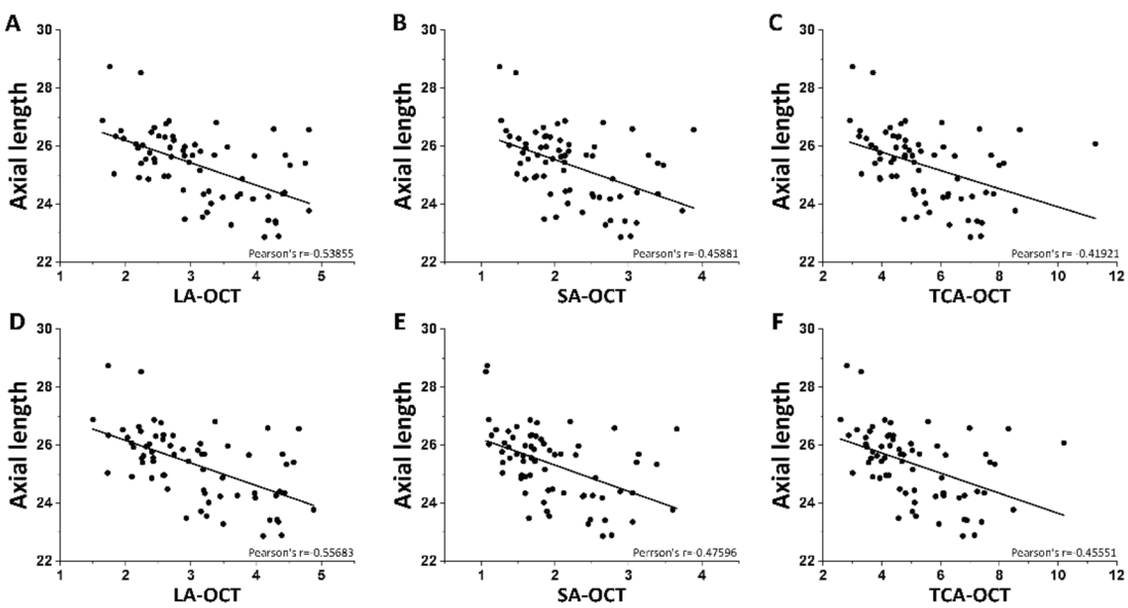

Figure 6 Scatter plots and fitting curves showing the correlations between area parameters and axial length (AL) A-C: Correlations between AL and LA-OCT, SA-OCT, and TCA-OCT from the VG200I; D-F: Correlations between AL and LA-OCT, SA-OCT, and TCA-OCT from the Triton. LA-OCT: Luminal area of the choroid calculated with the custom-designed algorithm on the OCT images; SA-OCT: Stromal area of the choroid calculated with the custom-designed algorithm on the OCT images; TCA-OCT: Total choroidal area calculated with the custom-designed algorithm on the OCT images; OCT: Optical coherence tomography.

repeatability and reproducibility between both image analysis methods. The measurements of various parameters, such as the LA, SA, and TCA, obtained from OCT images using both the VG200I and Triton also exhibited good repeatability and reproducibility. However, there was only moderate agreement between the Triton and VG200I in the CVI measured from OCT images and poor agreement for the CVI measured from OCTA images. Furthermore, both devices showed inconsistent agreement when the CVIs obtained with the two image analysis methods were compared.

Previous studies have assessed the repeatability and reproducibility in measuring the CVI using different OCT devices with custom software. Breher *et al*[32] and Sim *et al*[33] used custom software to calculate the CVI from OCT images obtained with a PlexElite 9000 and Spectralis, and both reported good repeatability and reproducibility.

Our study also revealed good repeatability and reproducibility in the measurements of middle and large vessel density in the choroid using both OCT devices. This study also revealed good repeatability and reproducibility of the CVI measured from OCTA images with built-in software, indicating that the collected images and different analysis methods were stable. However, in this study and previous studies, only the stability of static CVI measurements was investigated; however, choroidal blood flow can be easily influenced by various factors, such as accommodation and the circadian rhythm[17-18]. Further exploration of the stability of CVI measurements and changes in the CVI under the influence of such factors is necessary.

The agreement in the CVI-OCTA obtained from built-in software between the VG200I and Triton showed a large 95% LoA. Previous studies that measured retinal vessel density to explore the consistency between OCT devices also revealed poor consistency when built-in OCT software was used for quantification[34-36]. Studies by Lei *et al*[28] and Magrath *et al*[37], which used built-in OCTA software for region segmentation and custom software for quantifying the CVI, also reported poor consistency between devices. We speculate that differences in the quantization algorithms and artifact processing methods resulted in differing accuracy rates in identifying blood vessels are responsible for this poor consistency. First, the VG200I quantification algorithm calculates the CVI by identifying the lumen of large- and medium-sized vessels in B-scans through grayscale recognition, whereas the OCTA quantitative algorithm of the Triton employs a ratio-based method to measure motion contrast and thereby visualize blood vessel flow[38]. Second, the VG200I is equipped with an eye-tracking tool based on integrated confocal scanning laser ophthalmoscopy to eliminate eye motion artifacts, whereas the Triton uses the selective averaging of multiple B-scan combinations to suppress motion artifacts, which may interfere with the recognition of blood vessels in the images.

In contrast to the CVI-OCTA, the agreement in the CVI-OCT between the VG200I and Triton was relatively good, as was the consistency in the LA, SA, and TCA obtained from OCT images. Ma *et al*[39] also used custom software to segment and quantify OCT images and reported good consistency between the VG200D and Spectralis. In the analysis of the CVI-OCT, custom software was used to segment and quantify choroidal boundaries, resulting in the same ability to recognize blood vessels. The images obtained by the two devices were consistent, and both had high resolution, allowing the identical recognition of the LA and SA region after image binarization, resulting in good consistency in the measurement of the LA, SA, and TCA and, therefore, good consistency in the measurement of the CVI-OCT.

The agreement between OCT and OCTA in the measured CVI for both OCT devices was poor (ICC between -0.129 and 0.099). No previous study has explored the agreement between these two analytical methods. We believe that the main reason for the poor agreement is the difference in scanning method, producing different images and, thus, different blood vessel recognition results. OCT images consist of 18 or 12 circular A-scan scans centered on the macula, whereas OCTA images consist of vertical and horizontal parallel A-scan and B-scan scans. The CVIs calculated from the two images are therefore not comparable in terms of utility for clinical follow-up or scientific research.

The CVI-OCTA calculated with the Triton was positively correlated with AL, whereas the CVI-OCT and CVI-OCTA calculated with from the VG200I were not. Previous studies have been inconsistent in the reported correlation between the CVI and AL. Wu *et al*[24] analyzed vertical and horizontal scanning OCT images from adults with anisometropia and reported a negative correlation only between the vertical scanning CVI and AL. However, when the 18 images from all the scanning directions were combined to obtain the CVI of the whole central macular area with the same analysis method, a correlation between the CVI and AL was not identified in children with anisometropia[21]. Even when the same analysis method is used, the CVI and AL can have different relationships under different image acquisition modes. Different analysis methods for measuring the CVI also resulted in different correlations for the same subjects in this study. Although the correlation between the CVI-OCT and AL was not always consistent, there was a stable negative correlation between the SA, LA, and TCA and AL. In the study by Xu *et al*[40], subjects were given atropine at different concentrations and followed up for 1y. The results indicated that SA, LA, and TCA mediated approximately one-third of the effect of 1% atropine on myopia control, whereas no mediating effect was found for the CVI. Therefore, we speculate that the vascular area is more suitable for evaluating the relationship between the AL and choroidal perfusion than the CVI is.

There are several limitations in this study. First, we initially aimed to include four OCT devices (VG200I, DRI OCT Triton, PLEX Elite 9000, and RTVue XR Avanti) for comparison. However, the PLEX Elite 9000 is limited in that it can only obtain measurements when the pupil is enlarged after cycloplegia, which may affect the state of the choroid. Additionally, the images obtained from the RTVue XR Avanti were not sufficiently clear for analysis, so we ultimately included only two devices for CVI data analysis. Second, our study included young, healthy adults with narrow age ranges. As a result, we were unable to determine the impact of age and eye disease on the CVI or whether measuring the CVI in children can still yield good repeatability and reproducibility. The inclusion of adults as subjects allows only testing of the stability of the image analysis methodology and cannot represent the actual stability in clinical applications. Third, considering the clinical significance of the peripapillary region in eye health research, the lack of evaluation of this region using OCT(A) is noted. While previous studies have demonstrated good repeatability of peripapillary perfusion measurements, the agreement across different devices and analysis methods remains unexplored[41]. We proposed future research to assess the consistency of peripapillary OCT measurements across different devices represents a logical and

necessary step to enhance the reliability and standardization of OCT. This will help address potential variability and ensure the robustness of scientific findings.

In conclusion, both OCT devices exhibited good repeatability and reproducibility in measuring the CVI from both OCT and OCTA images. The consistency in the LA, SA, and TCA measured from OCT images and in the CVI-OCT between devices was good, but the consistency in the CVI-OCTA was poor. Given the poor consistency between the CVI-OCTA and CVI-OCT measured with the VG200 and Triton, we consider the CVI-OCT from the Triton and the CVI-OCT from the VG200 to be relatively reliable; however, the reliability regarding the CVI-OCTA still needs to be further verified. Only the CVI-OCTA from the Triton was positively correlated with AL, whereas the CVI-OCT from both devices and the CVI-OCTA from the VG200I were not. According to our results, the CVI is not suitably stable for exploring relationships with AL. For the data from different devices to be comparable or suitable for use in follow-up comparisons, the same quantification calculation method and region segmentation approach should be employed.

ACKNOWLEDGEMENTS

Authors' Contributions: Huang YY and Bao JH had full access to all the data in the study and take responsibility for the integrity of the data and the accuracy of the data analysis. Zhong MH and Zhang JL share co-first authorship. Concept and design: Bao JH, Huang YY; Acquisition, analysis, or interpretation of data: Zhong MH, Zhang JL, Yu KX, Fan SQ, Li X, Chen H, Bao JH, Huang YY; Drafting of the manuscript: Huang YY, Zhong MH; Critical revision of the manuscript for important intellectual content: Zhong MH, Zhang JL, Yu KX, Fan SQ, Li X, Chen H, Bao JH, Huang YY; Statistical analysis: Zhong MH, Zhang JL; Funding acquisition: Bao JH. All authors read and approved the final manuscript.

Availability of Data and Materials: The datasets used and analyzed for the present study are available from the corresponding authors upon reasonable request.

Artificial Intelligence Statement Disclosure: During the preparation of this work, generative AI or AI-assisted technologies were not used in this article.

Foundations: Supported by the National Key Research and Development Program of China (No.2022YFC3502503); the Medical and Health Science and Technology Project of the Zhejiang Provincial Health Commission of China (No.2022PY072).

Conflicts of Interest: Zhong MH, None; **Zhang JL,** None; **Yu KX,** None; **Fan SQ,** None; **Li X,** None; **Chen H,** None; **Bao JH,** None; **Huang YY,** None.

REFERENCES

1 Wu H, Chen W, Zhao F, *et al*. Scleral hypoxia is a target for myopia control. *Proc Natl Acad Sci U S A* 2018;115(30): e7091-e7100.

2 Keskin Ç, Dilekçi ENA, Üçgül AY, *et al*. Choroidal vascularity index as a predictor for the development of retinopathy in diabetic patients. *J Endocrinol Investig* 2024;47(5):1175-1180.

3 Shin DY, Hong KE, Lee NY, *et al*. Association of choroidal blood flow with autonomic dysfunction in patients with normal tension glaucoma. *Sci Rep* 2022;12:5136.

4 Robbins CB, Thompson AC, Bhullar PK, *et al*. Characterization of retinal microvascular and choroidal structural changes in Parkinson disease. *JAMA Ophthalmol* 2021;139(2):182.

5 Spaide RF, Fujimoto JG, Waheed NK, *et al*. Optical coherence tomography angiography. *Prog Retin Eye Res* 2018;64:1-55.

6 Tang Y, Zhao Y, Wang QY, *et al*. Advances in choroid-glaucoma structural-functional correlations using swept-source optical coherence tomography. *Photodiagn Photodyn Ther* 2025;54:104627.

7 Maruko I, Spaide RF, Koizumi H, *et al*. Choroidal blood flow visualization in high myopia using a projection artifact method in optical coherence tomography angiography. *Retina* 2017;37(3):460-465.

8 Zhang QQ, Zheng F, Motulsky EH, *et al*. A novel strategy for quantifying choriocapillaris flow voids using swept-source OCT angiography. *Invest Ophthalmol Vis Sci* 2018;59(1):203.

9 Laíns I, Wang JC, Cui Y, *et al*. Retinal applications of swept source optical coherence tomography (OCT) and optical coherence tomography angiography (OCTA). *Prog Retin Eye Res* 2021;84:100951.

10 Devarajan K, Sim R, Chua J, *et al*. Optical coherence tomography angiography for the assessment of choroidal vasculature in high myopia. *Br J Ophthalmol* 2020;104(7):917-923.

11 Liu XT, Lin ZY, Wang FF, *et al*. Choroidal thickness and choriocapillaris vascular density in myopic anisometropia. *Eye Vis (Lond)* 2021;8(1):48.

12 Wang YY, Chen SS, Lin J, *et al*. Vascular changes of the choroid and their correlations with visual acuity in pathological myopia. *Invest Ophthalmol Vis Sci* 2022;63(12):20.

13 Kee AR, Yip VCH, Tay ELT, *et al*. Comparison of two different optical coherence tomography angiography devices in detecting healthy versus glaucomatous eyes–an observational cross-sectional study. *BMC Ophthalmol* 2020;20(1):440.

14 Querques G, Borrelli E, Sacconi R, *et al*. Functional and morphological changes of the retinal vessels in Alzheimer's disease and mild cognitive impairment. *Sci Rep* 2019;9:63.

15 Robbins CB, Grewal DS, Thompson AC, *et al*. Choroidal structural analysis in Alzheimer disease, mild cognitive impairment, and cognitively healthy controls. *Am J Ophthalmol* 2021;223:359-367.

16 Chen SS, Zheng G, Yu XL, *et al*. Impact of penetration and image analysis in optical coherence tomography on the measurement of choroidal vascularity parameters. *Retina* 2022;42(10):1965-1974.

17 Ulaganathan S, Read SA, Collins MJ, *et al*. Daily axial length and choroidal thickness variations in young adults: Associations with light exposure and longitudinal axial length and choroid changes. *Exp Eye Res* 2019;189:107850.

18 Chakraborty R, Read SA, Collins MJ. Hyperopic defocus and diurnal changes in human choroid and axial length. *Optom Vis Sci* 2013;90(11):1187-1198.

19 Zheng G, Jiang YF, Shi C, *et al*. Deep learning algorithms to segment and quantify the choroidal thickness and vasculature in swept-source optical coherence tomography images. *J Innov Opt Health Sci* 2021;14:2140002.

20 Park JW, Suh MH, Agrawal R, *et al*. Peripapillary choroidal vascularity index in glaucoma—a comparison between spectral-domain OCT and OCT angiography. *Invest Ophthalmol Vis Sci* 2018;59(8):3694.

21 Wu H, Zhang GY, Shen MX, *et al*. Assessment of choroidal vascularity and choriocapillaris blood perfusion in anisomyopic adults by SS-OCT/OCTA. *Invest Ophthalmol Vis Sci* 2021;62(1):8.

22 Hwang YH, Kim YY. Macular thickness and volume of myopic eyes measured using spectral-domain optical coherence tomography. *Clin Exp Optom* 2012;95(5):492-498.

23 Vaghefi E, Hill S, Kersten HM, *et al*. Quantification of optical coherence tomography angiography in age and age-related macular degeneration using vessel density analysis. *Asia Pac J Ophthalmol (Phila)* 2020;9(2):137-143.

24 Wu H, Xie Z, Wang PQ, *et al*. Differences in retinal and choroidal vasculature and perfusion related to axial length in pediatric anisomyopes. *Invest Ophthalmol Vis Sci* 2021;62(9):40.

25 Luo H, Sun JF, Chen L, *et al*. Compartmental analysis of three-dimensional choroidal vascularity and thickness of myopic eyes in young adults using SS-OCTA. *Front Physiol* 2022;13:916323.

26 Wang YY, Liu MQ, Xie Z, *et al*. Choroidal circulation in 8- to 30-year-old Chinese, measured by SS-OCT/OCTA: relations to age, axial length, and choroidal thickness. *Invest Ophthalmol Vis Sci* 2023;64(7):7.

27 Qiao YL, Cheng D, Zhu XY, *et al*. Characteristics of the peripapillary structure and vasculature in patients with myopic anisometropia. *Trans Vis Sci Tech* 2023;12(10):16.

28 Lei JQ, Pei C, Wen C, *et al*. Repeatability and reproducibility of quantification of superficial peri-papillary capillaries by four different optical coherence tomography angiography devices. *Sci Rep* 2018;8:17866.

29 Zhang JY, Tang FY, Cheung CY, *et al*. Different effect of media opacity on vessel density measured by different optical coherence tomography angiography algorithms. *Trans Vis Sci Tech* 2020;9(8):19.

30 Ataş F, Kaya M, Ayhan Z, *et al*. Evaluation of choroidal vascularity index in systemic sclerosis patients. *Photodiagn Photodyn Ther* 2023;41:103297.

31 Wang XH, Li R, Chen JY, *et al*. Choroidal vascularity index (CVI)-Net-based automatic assessment of diabetic retinopathy severity using CVI in optical coherence tomography images. *J Biophotonics* 2023;16(6):e202200370.

32 Breher K, Terry L, Bower T, *et al*. Choroidal biomarkers: a repeatability and topographical comparison of choroidal thickness and choroidal vascularity index in healthy eyes. *Trans Vis Sci Tech* 2020;9(11):8.

33 Sim DA, Keane PA, Mehta H, *et al*. Repeatability and reproducibility of choroidal vessel layer measurements in diabetic retinopathy using enhanced depth optical coherence tomography. *Invest Ophthalmol Vis Sci* 2013;54(4):2893.

34 Corvi F, Cozzi M, Barbolini E, *et al*. Comparison between several optical coherence tomography angiography devices and indocyanine green angiography of choroidal neovascularization. *Retina* 2020;40(5):873-880.

35 Mihailovic N, Brand C, Lahme L, *et al*. Repeatability, reproducibility and agreement of foveal avascular zone measurements using three different optical coherence tomography angiography devices. *PLoS One* 2018;13(10):e0206045.

36 Corvi F, Corradetti G, Parrulli S, *et al*. Comparison and repeatability of high resolution and high speed scans from spectralis optical coherence tomography angiography. *Trans Vis Sci Tech* 2020;9(10):29.

37 Magrath GN, Say EAT, Sioufi K, *et al*. Variability in foveal avascular zone and capillary density using optical coherence tomography angiography machines in healthy eyes. *Retina* 2017;37(11):2102-2111.

38 Stanga PE, Tsamis E, Papayannis A, *et al*. Swept-source optical coherence tomography angio™ (Topcon Corp, Japan): technology review. *Dev Ophthalmol* 2016;56:13-17.

39 Ma FY, Bai YF, Duan JL, *et al*. Validation of reliability, repeatability and consistency of three-dimensional choroidal vascular index. *Sci Rep* 2024;14:1576.

40 Xu HN, Ye LY, Peng YJ, *et al*. Potential choroidal mechanisms underlying atropine's antimyopic and rebound effects: a mediation analysis in a randomized clinical trial. *Invest Ophthalmol Vis Sci* 2023;64(4):13.

41 Fang DQ, Mai XT, Cheung CY, *et al*. Repeatability, interocular correlation and agreement of optic nerve head vessel density in healthy eyes: a swept-source optical coherence tomographic angiography study. *Int J Ophthalmol* 2024;17(5):896-903.